# Internal structure of acceptor-bound excitons in wide-band-gap wurtzite semiconductors

Bernard Gil
*Université Montpellier II,Groupe d'Etude des Semiconducteurs , UMR CNRS 5650, Case Courrier 074, F-34095 Montpellier Cedex 5, France*

Pierre Bigenwald
*Clermont Université, Université Blaise Pascal, LASMEA, BP 10448, F-63000 Clermont Ferrand, France and CNRS, UMR 6602, LASMEA, F-63177 Aubière Cedex, France*

Plamen P. Paskov and Bo Monemar
*Linköping University, Department of Physics, Chemistry & Biology, S-58183 Linkoping, Sweden*
(Received 12 October 2009; revised manuscript received 14 December 2009; published 10 February 2010)

We describe the internal structure of acceptor-bound excitons in wurtzite semiconductors. Our approach consists in first constructing, in the context of angular momentum algebra, the wave functions of the two-hole system that fulfill Pauli's exclusion's principle. Second, we construct the acceptor-bound exciton states by adding the electron states in a similar manner that two-hole states are constructed. We discuss the optical selection rules for the acceptor-bound exciton recombination. Finally, we compare our theory with experimental data for CdS and GaN. In the specific case of CdS for which much experimental information is available, we demonstrate that, compared with cubic semiconductors, the sign of the short-range hole-exchange interaction is reversed and more than one order of magnitude larger. The whole set of data is interpreted in the context of a large value of the short-range hole-exchange interaction $\Xi_0=3.4\pm0.2$ meV. This value dictates the splitting between the ground-state line $I_1$ and the other transitions. The values we find for the electron-hole spin-exchange interaction and of the crystal-field splitting of the two-hole state are, respectively, $-0.4\pm0.1$ and $0.2\pm0.1$ meV. In the case of GaN, the experimental data for the acceptor-bound excitons in the case of Mg and Zn acceptors, show more than one bound-exciton line. We discuss a possible assignment of these states.

DOI: 10.1103/PhysRevB.81.085211 PACS number(s): 71.35.Cc, 71.55.−i, 71.70.Gm

## I. INTRODUCTION

The radiative recombination of bulk semiconductors is, in general, dominated by excitons localized to impurities, impurity complexes, or fluctuations of the crystal potential that trap charge carriers, rather than by free-exciton fluorescence.[1] The free-exciton recombination, even in direct band-gap semiconductors, has a "forbidden nature" in momentum space, related with the difficulty to fulfill wave-vector momentum-conservation criteria: the *large* wave vector of the freely propagating exciton in the crystal has to be transformed into a *small* photon wave vector propagating out of the material. This process is not straightforward and may be interpreted in terms of the complex interaction of the electromagnetic field with the crystal states via the exciton-polariton picture. The weakness of the free-exciton fluorescence can then be interpreted in terms of radiative decay times, exciton-photon scattering processes, and photon density of states.[2] This momentum-conservation rule is relaxed for localized excitons, as in the case of impurity-bound excitons, when the exciton or carrier wave vectors are reduced by localization. The value of the radiative decay time of the bound exciton is decreased with respect to the value of the "radiative decay time of the free exciton." This leads to stronger photoluminescence (PL) peaks than free-exciton ones. The photoluminescence intensity of bound excitons is also reinforced by thermalization effects; localization leads to a quantum state of lower energy than the energy of the free exciton and thus favors population of these low-energy states at low temperatures. The near band-gap photoluminescence features of semiconductors therefore show a complicated structure with, from high to low energies, the free exciton, donor-bound exciton, acceptor-bound exciton, other defect bound-exciton lines, excitons bound to pair defects, or more complex clusters. Phonon-assisted recombination may also occur, further complicating the picture. Localization of a free exciton occurs via a long-range potential interaction (this is typical of hydrogenic impurities) and/or via a medium-range or short-range potential. Both contributions are, in principle, a signature of the nature of the localizing potential. Photoluminescence can be used to probe the doping of a semiconductor and eventually to discriminate localization centers.[1]

The real situation with the electronic structure of bound excitons in crystalline semiconductors is much more complicated. Electrons and holes have their respective effective masses related to the real band structure, and free excitons can be viewed as analogs of positronium atoms rather than as analogs of hydrogen atoms. This influences the fine-structure splitting of exciton states. The situation is even more complicated in semiconductors with the *p*-type symmetry of the valence band. The hole has to be treated in the context of its sixfold (including spin) symmetry. Therefore, bound-exciton physics cannot be handled from a transfer of the physics of small electron atoms.[3] We have recently reviewed the physics of donor-bound excitons in cubic and wurtzite semiconductors.[4] We could, by using this model, properly interpret the symmetry of two-electron transitions (related to an Auger-type recombination process that promotes the residual electron into an excited state of the donor).[4,5]

 

This paper addresses the internal structure of acceptor-bound excitons in wurtzite semiconductors. Careful examination of the literature has not revealed any full theoretical treatment of this problem in semiconductors, including the fundamental valence-band states and the spin-orbit split-off ones. The case of cubic (zinc-blende) semiconductors previously addressed by many groups[6] can be easily obtained in the angular momentum treatment that follows by increasing the symmetry of the problem. This may be realized via cancellation of the crystal-field splitting parameter and by giving an identical value to two matrix elements of the spin-orbit coupling in the valence band. Below, the electronic structure of acceptor-bound excitons will be developed stepwise. First, we describe the valence-band hole states, with relevance to the single-particle effective-mass bound hole states in the acceptor potential, derived from the valence-band top. The next step is the addition of a second hole to the potential, i.e., a description of a bound two-hole state, where the hole-hole exchange interaction is included. Finally, the outer electron is added, completing the bound exciton, in the spirit of the classical Thomas-Hopfield model.[7] At this stage, the effects of the electron-hole exchange interaction are introduced.

Our model is further applied to CdS where proper experimental data exist in the literature.[7,8] We demonstrate that the previous interpretation of the data is inconsistent with the predictions of group theory and with the valence-band structure of CdS. We propose a new one that is consistent with the experimentally established symmetry of the acceptor-bound exciton states. For GaN, the experimental data for the acceptor-bound excitons in the case of Mg and Zn acceptors, show splitting into more than one bound-exciton ground state. We discuss a possible assignment of these states.

The paper is organized as follows. Section II is dedicated to recall some basic elements of the valence-band physics of wurtzite semiconductors. Then, in Sec. III, we construct the wave functions of the two-hole system that fulfill Pauli's exclusion's principle. In Sec. IV, we construct the acceptor-bound exciton states and discuss the optical selection rules for the acceptor-bound exciton recombination. Finally, we compare our theory with experimental data for CdS and GaN.

## II. HOLE STATES (VALENCE-BAND STATES) IN WURTZITE SEMICONDUCTORS

In this section, we recall some of the basic elements required to describe the physics of holes in wurtzite semiconductors at the zone center, in the context of invariants theory. We point out that a description of bound acceptor states and acceptor-bound exciton states also involves consideration of the acceptor potential localizing the carriers. As discussed previously,[1] an effective-masslike approach is sufficient to describe the proper symmetry of shallow acceptor or bound-exciton states, and the relevant fine-structure splitting. Any attempt to calculate the binding energies of the particles necessarily involves accounting for the detailed shape of the localization potential, and is a very difficult problem for bound excitons, as described in Ref. 1. In the treatment below, we therefore do not expect to accurately represent the absolute energies of the bound-exciton states but the symmetry, fine-structure splitting, and classification of the bound states are expected to be properly obtained, as discussed in the original paper by Thomas and Hopfield.[7]

In a spinless description, the valence-band states are represented in the $B_0$ basis in terms of the following spherical harmonics:

$$|1\rangle = \left| -\frac{x+iy}{\sqrt{2}} \right\rangle,$$

$$|0\rangle = |z\rangle,$$

$$|\bar{1}\rangle = \left| \frac{x-iy}{\sqrt{2}} \right\rangle. \tag{1}$$

These states are split by the wurtzite crystal field and the spectral picture is obtained phenomenologically by application of the following operator:[9]

$$H_0 = \Delta_1 L_z^2, \tag{2}$$

where $\Delta_1$ is the crystal-field energy and $L_z$ is the $z$ component of the angular momentum. The $z$ direction is chosen to be parallel to the $c$ axis of the crystal. The spectral dependence of the valence-band states, including spin is accounted for by the following operator:[10]

$$H_1 = \Delta_1 L_z^2 + \Delta_2 (L_x \sigma_x + L_y \sigma_y) + \Delta_3 L_z \sigma_z, \tag{3}$$

where $\Delta_2$ and $\Delta_3$ are spin-orbit energy parameters and $\sigma_i$ are components of the spin operators. The simplest form of this Hamiltonian is written as follows:

$$H_1 = H_{\text{one-hole}}$$

$$= \begin{array}{c|cccccc} & |1\rangle\uparrow & |\bar{1}\rangle\downarrow & |1\rangle\downarrow & |0\rangle\uparrow & |\bar{1}\rangle\uparrow & |0\rangle\downarrow \\ \hline |1\rangle\uparrow & \Delta_1+\Delta_2 & 0 & 0 & 0 & 0 & 0 \\ |\bar{1}\rangle\downarrow & 0 & \Delta_1+\Delta_2 & 0 & 0 & 0 & 0 \\ |1\rangle\downarrow & 0 & 0 & \Delta_1-\Delta_2 & \sqrt{2}\Delta_3 & 0 & 0 \\ |0\rangle\uparrow & 0 & 0 & \sqrt{2}\Delta_3 & 0 & 0 & 0 \\ |\bar{1}\rangle\uparrow & 0 & 0 & 0 & 0 & \Delta_1-\Delta_2 & \sqrt{2}\Delta_3 \\ |0\rangle\downarrow & 0 & 0 & 0 & 0 & \sqrt{2}\Delta_3 & 0 \end{array}, \tag{4}$$

where $\uparrow$ and $\downarrow$ denote the two spin components of the holes. The eigenvalues and their corresponding eigenvectors are doubly degenerate and given by

$$E_9 = \Delta_1 + \Delta_2 \tag{5}$$

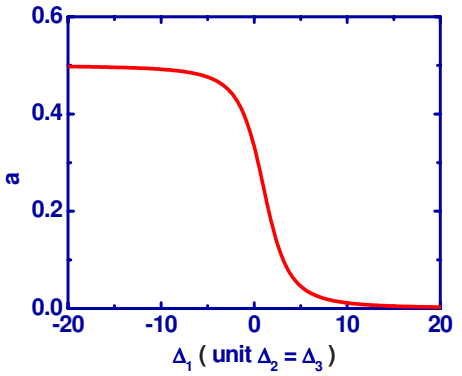


FIG. 1. (Color online) Coupling parameter $a$ for wave functions of $\Gamma_7$ valence-band states (distribution of the $E_7^1$ valence-band states in terms of $|0\rangle$) as a function of the crystal-field splitting in units of the spin-orbit interaction parameter.

with $V_9$ eigenvectors being $|1\rangle\uparrow$ and $|\bar{1}\rangle\downarrow$, that we write $\begin{pmatrix}|1\rangle\uparrow\\ |\bar{1}\rangle\downarrow\end{pmatrix}$. The two-row matrix representation is here introduced to give the two eigenvectors using a compact notation, i.e., one row for one eigenvector,

$$E_7^1 = \frac{\Delta_1 - \Delta_2}{2} + \sqrt{\left(\frac{\Delta_1 - \Delta_2}{2}\right)^2 + 2\Delta_3^2} \tag{6}$$

with $V_7^1$ eigenvectors being

$$V_7^1 = \sqrt{1-a^2}\begin{pmatrix}|1\rangle\downarrow\\ |\bar{1}\rangle\uparrow\end{pmatrix} + a\begin{pmatrix}|0\rangle\uparrow\\ |0\rangle\downarrow\end{pmatrix}, \tag{7}$$

$$E_7^2 = \frac{\Delta_1 - \Delta_2}{2} - \sqrt{\left(\frac{\Delta_1 - \Delta_2}{2}\right)^2 + 2\Delta_3^2} \tag{8}$$

with $V_7^2$ eigenvectors being

$$V_7^2 = a\begin{pmatrix}|1\rangle\downarrow\\ |\bar{1}\rangle\uparrow\end{pmatrix} - \sqrt{1-a^2}\begin{pmatrix}|0\rangle\uparrow\\ |0\rangle\downarrow\end{pmatrix}. \tag{9}$$

In Eqs. (7)–(9), the parameter $a$ is given by

$$a = \frac{\sqrt{2}\Delta_3}{\sqrt{\left[\frac{\Delta_1 - \Delta_2}{2} - \sqrt{\left(\frac{\Delta_1 - \Delta_2}{2}\right)^2 - 2\Delta_3^2}\right]^2 + 2\Delta_3^2}}. \tag{10}$$

The evolution of $a$ with $(\Delta_1/\Delta_2)$ in the particular case where $\Delta_2 = \Delta_3$ is plotted in Fig. 1. The eigenvalues $E_9$ (respectively, $E_7^1$) are associated eigenvectors of the $\Gamma_9$ (respectively, $\Gamma_7$) symmetry. In the symmetry-inappropriate context of a band to band description of the optical transitions at the band-gap energy of the wurtzite semiconductors (e.g., GaN), they, respectively, correspond to the commonly discussed $A$, $B$, and $C$ transitions.[11,12] The two-component nature of the $\Gamma_7$ wave functions indicates that the band to band transitions are allowed in both $\sigma(\mathbf{E}\perp\mathbf{c})$ and $\pi(\mathbf{E}\|\mathbf{c})$ polarizations with relative oscillator strength being proportional to the square of their expansion components along $|1\rangle$, $|\bar{1}\rangle$, and $|0\rangle$ spinless valence-band states.[13]

Including the two components of the spin, the valence-band states are sometimes expressed in the basis set of spherical angular momenta. Often a $\{J, m_J\}$ representation is used, where $J$ is the total angular momentum and $m_J$ its $z$ projection,

$$\begin{pmatrix}\left|\frac{3}{2},\frac{3}{2}\right\rangle\\ \left|\frac{3}{2},\frac{1}{2}\right\rangle\\ \left|\frac{3}{2},-\frac{1}{2}\right\rangle\\ \left|\frac{3}{2},-\frac{3}{2}\right\rangle\\ \left[\frac{1}{2},\frac{1}{2}\right)\\ \left[\frac{1}{2},-\frac{1}{2}\right)\end{pmatrix} = \begin{pmatrix}\left|\frac{3}{2}\right\rangle\\ \left|\frac{1}{2}\right\rangle\\ \left|-\frac{1}{2}\right\rangle\\ \left|-\frac{3}{2}\right\rangle\\ \left[\frac{1}{2}\right)\\ \left[-\frac{1}{2}\right)\end{pmatrix} = \begin{pmatrix}1 & 0 & 0 & 0 & 0 & 0\\ 0 & \sqrt{\frac{2}{3}} & 0 & \frac{1}{\sqrt{3}} & 0 & 0\\ 0 & 0 & \frac{1}{\sqrt{3}} & 0 & \sqrt{\frac{2}{3}} & 0\\ 0 & 0 & 0 & 0 & 0 & 1\\ 0 & -\frac{1}{\sqrt{3}} & 0 & \sqrt{\frac{2}{3}} & 0 & 0\\ 0 & 0 & -\sqrt{\frac{2}{3}} & 0 & \frac{1}{\sqrt{3}} & 0\end{pmatrix}\begin{bmatrix}|1\rangle\uparrow\\ |0\rangle\uparrow\\ |\bar{1}\rangle\uparrow\\ |1\rangle\downarrow\\ |0\rangle\downarrow\\ |\bar{1}\rangle\downarrow\end{bmatrix}. \tag{11}$$

Note the use of round bras for representing the spin-orbit split-off states. The one-hole Hamiltonian [Eq. (4)] now rewrites as

$$H_{\text{one-hole}} = \begin{array}{c} \left|\pm\frac{3}{2}\right\rangle \\ \Delta_1+\Delta_2 \\ 0 \\ 0 \end{array} \begin{array}{c} \left|\pm\frac{1}{2}\right\rangle \\ 0 \\ \frac{\Delta_1-\Delta_2+4\Delta_3}{3} \\ \frac{\sqrt{2}(\Delta_1-\Delta_2+\Delta_3)}{3} \end{array} \begin{array}{c} \left[\pm\frac{1}{2}\right) \\ 0 \\ \frac{\sqrt{2}(\Delta_1-\Delta_2+\Delta_3)}{3} \\ \frac{2\Delta_1-2\Delta_2-4\Delta_3}{3} \end{array}. \tag{12}$$

## III. TWO-HOLE STATES

For two Fermi particles having angular momentum $J_1$ and $J_2$, the wave function of total angular momentum $J$ in nonequivalent orbits is[14]

$$|J,m\rangle = \frac{1}{\sqrt{2}}\sum_{\mu} C(J_1J_2J;\mu,m-\mu) \times \begin{vmatrix} |J_1,\mu\rangle^1 & |J_1,\mu\rangle^2 \\ |J_2,m-\mu\rangle^1 & |J_2,m-\mu\rangle^2 \end{vmatrix}, \tag{13}$$

where $C$ are the classical Clebsch-Gordon coefficients for one particle,[15]

$$|J,m\rangle = \sum_{\mu} C(J_1J_2J;m,m-\mu)|J_1,\mu\rangle|J_2,m-\mu\rangle \tag{14}$$

and $m$ is the projection of the total angular momentum $J$; $m$, *integer*, runs from $-J$ to $J$.

The two-hole states can be built by coupling either two $J=3/2$ hole states, two $J=1/2$ hole states, or a $J=3/2$ hole state with a $J=1/2$ hole state. Coupling of two $J=3/2$ hole states is the model used for cubic zinc-blende semiconductors such as GaAs and InP.[6] In GaAs and InP, this restriction is possible in correlation with the huge value of the spin-orbit interaction $\Delta_{SO}=3\Delta_2=3\Delta_3$, respectively, equal to 340 and 120 meV compared to the exciton binding energy $E_B$ =4.3 and 5.2 meV, respectively.[16] Then, the low-energy levels are the only nonresonant ones and the strength of the coupling of the fundamental acceptor states with the spin-orbit split-off one is very weak. This is not the case in wurtzite semiconductors (GaN, ZnO), displaying simultaneously a crystal-field-induced splitting of the fourfold $J=3/2$ states and a weak spin-orbit interaction.

### A. Two-hole wave functions in the case of coupling of two identical holes

According to the Pauli symmetry principle, the two-hole states display antisymmetric behavior by particle exchange. Following group-theory arguments, in terms of angular momentum algebra, the relevant states are $|2,m_2\rangle$ and $|0,0\rangle$ born from the coupling of two $J=3/2$ holes, and $[0,0)$ from the coupling of two $J=1/2$ holes. These eigenvectors are expressed using Slater determinants where the two holes are labeled using superscript numbers 1 and 2, and their wave functions are referenced using triangular or round bras depending on whether they originate from $J=3/2$ state or from $J=1/2$ state (spin-orbit split-off state). For the sake of completeness, we also give their symmetry in terms of the reducible representations $\Gamma_i$ of the $C_{6v}$ point group. Note the use of superscript to label the irreducible representations when a given symmetry appears several times,

$$[\Gamma_1^1) = [0,0) = \frac{1}{\sqrt{2}} \begin{vmatrix} \left[-\frac{1}{2}\right)^1 & \left[-\frac{1}{2}\right)^2 \\ \left[\frac{1}{2}\right)^1 & \left[\frac{1}{2}\right)^2 \end{vmatrix}, \tag{15}$$

$$|\Gamma_1^2\rangle = |0,0\rangle = \frac{1}{2} \begin{vmatrix} \left|-\frac{1}{2}\right\rangle^1 & \left|-\frac{1}{2}\right\rangle^2 \\ \left|\frac{1}{2}\right\rangle^1 & \left|\frac{1}{2}\right\rangle^2 \end{vmatrix} - \frac{1}{2} \begin{vmatrix} \left|-\frac{3}{2}\right\rangle^1 & \left|-\frac{3}{2}\right\rangle^2 \\ \left|\frac{3}{2}\right\rangle^1 & \left|\frac{3}{2}\right\rangle^2 \end{vmatrix}, \tag{16}$$

$$|\Gamma_1^3\rangle = |2,0\rangle = -\frac{1}{2} \begin{vmatrix} \left|-\frac{1}{2}\right\rangle^1 & \left|-\frac{1}{2}\right\rangle^2 \\ \left|\frac{1}{2}\right\rangle^1 & \left|\frac{1}{2}\right\rangle^2 \end{vmatrix} - \frac{1}{2} \begin{vmatrix} \left|-\frac{3}{2}\right\rangle^1 & \left|-\frac{3}{2}\right\rangle^2 \\ \left|\frac{3}{2}\right\rangle^1 & \left|\frac{3}{2}\right\rangle^2 \end{vmatrix}, \tag{17}$$

$$|\Gamma_5^{1\pm}\rangle = |2,\pm 1\rangle = \pm\frac{1}{\sqrt{2}} \begin{vmatrix} \left|\pm\frac{3}{2}\right\rangle^1 & \left|\pm\frac{3}{2}\right\rangle^2 \\ \left|\mp\frac{1}{2}\right\rangle^1 & \left|\mp\frac{1}{2}\right\rangle^2 \end{vmatrix}, \tag{18}$$

$$|\Gamma_6^{1\pm}\rangle = |2,\pm 2\rangle = \pm\frac{1}{\sqrt{2}} \begin{vmatrix} \left|\pm\frac{3}{2}\right\rangle^1 & \left|\pm\frac{3}{2}\right\rangle^2 \\ \left|\mp\frac{1}{2}\right\rangle^1 & \left|\pm\frac{1}{2}\right\rangle^2 \end{vmatrix}. \tag{19}$$

It is worthwhile noticing that, except for $[\Gamma_1^1)$, the two-hole states are built from both $\Gamma_9|\pm\frac{3}{2}\rangle$ and $\Gamma_7|\pm\frac{1}{2}\rangle$ holes.

### B. Wave functions for the coupling of $J=3/2$ hole with $J=1/2$ hole

When the angular momentum of the second particle ($J_2$) is a spin (or any half integer), the total angular momentum for the two-particle system is $J_1+1/2$ or $J_1-1/2$ and the eigenvectors are given by

$$\left|J_1+\frac{1}{2},m\right\rangle=\sqrt{\frac{J_1+m+1/2}{2J_1+1}}\left|J_1,m-\frac{1}{2}\right\rangle\left|\frac{1}{2},\frac{1}{2}\right\rangle+\sqrt{\frac{J_1-m+1/2}{2J_1+1}}\left|J_1,m+\frac{1}{2}\right\rangle\left|\frac{1}{2},-\frac{1}{2}\right\rangle, \tag{20}$$

$$\left|J_1-\frac{1}{2},m\right\rangle=-\sqrt{\frac{J_1-m+1/2}{2J_1+1}}\left|J_1,m-\frac{1}{2}\right\rangle\left|\frac{1}{2},\frac{1}{2}\right\rangle+\sqrt{\frac{J_1+m+1/2}{2J_1+1}}\left|J_1,m+\frac{1}{2}\right\rangle\left|\frac{1}{2},-\frac{1}{2}\right\rangle. \tag{21}$$

In our case, the first particle has an angular momentum $J_1=3/2$ with eigenstates $|3/2,m_{3/2}\rangle^1$ while the second particle has an angular momentum $J_2=1/2$ with eigenstates $[1/2,m_{1/2})^2$. Therefore, the eigenvectors are

$$|\Gamma_6^{2\pm}\rangle=|2,\pm 2\rangle'=\left|\pm\frac{3}{2}\right\rangle^1\left[\pm\frac{1}{2}\right)^2, \tag{22}$$

$$|\Gamma_5^{2\pm}\rangle=|2,\pm 1\rangle'=\frac{1}{2}\left[\sqrt{3}\left|\pm\frac{1}{2}\right\rangle^1\left[\pm\frac{1}{2}\right)^2+\left|\pm\frac{3}{2}\right\rangle^1\left[\mp\frac{1}{2}\right)^2\right], \tag{23}$$

$$|\Gamma_1^4\rangle=|2,0\rangle'=\frac{1}{\sqrt{2}}\left[\left|-\frac{1}{2}\right\rangle^1\left[\frac{1}{2}\right)^2+\left|\frac{1}{2}\right\rangle^1\left[-\frac{1}{2}\right)^2\right], \tag{24}$$

$$|\Gamma_5^{3\pm}\rangle=|1,\pm 1\rangle=-\frac{1}{2}\left[\left|\pm\frac{1}{2}\right\rangle^1\left[\pm\frac{1}{2}\right)^2-\sqrt{3}\left|\pm\frac{3}{2}\right\rangle^1\left[\mp\frac{1}{2}\right)^2\right], \tag{25}$$

$$|\Gamma_1^5\rangle=|1,0\rangle=-\frac{1}{\sqrt{2}}\left[\left|-\frac{1}{2}\right\rangle^1\left[\frac{1}{2}\right)^2-\left|\frac{1}{2}\right\rangle^1\left[-\frac{1}{2}\right)^2\right]. \tag{26}$$

Note that, for $J=2$, vectors are primed in order to avoid confusion with the preceding series.

### C. Matrix representation of the two-hole Hamiltonian in the angular momentum representation

The matrix elements of the two-hole Hamiltonian are obtained as functions of the one-hole Hamiltonian [Eq. (12)] as follows:

$$\int\int \varphi_x^{1*}\varphi_y^{2*}H_{\text{two-hole}}\varphi_u^1\varphi_v^2 d^3r^1 d^3r^2=\delta_{yv}\int \varphi_x^{1*}H_1\varphi_u^1 d^3r^1+\delta_{xu}\int \varphi_y^{2*}H_2\varphi_v^2 d^3r^2 \tag{27}$$

or in Dirac notation

$$\langle\varphi_x^1\varphi_y^2|H_{\text{two-hole}}|\varphi_u^1\varphi_v^2\rangle=\langle\varphi_x^1|H_1|\varphi_u^1\rangle\langle\varphi_y^2|\varphi_v^2\rangle+\langle\varphi_y^2|H_2|\varphi_v^2\rangle\langle\varphi_x^1||\varphi_u^1\rangle=\langle\varphi_x|H|\varphi_u\rangle\delta_{yv}+\langle\varphi_y|H|\varphi_v\rangle\delta_{xu}. \tag{28}$$

Here the $H_i$ are the one-hole Hamiltonians, the $\varphi_\beta^\alpha$'s are the total wave functions (including spin) of the hole labeled in terms of particle ($\alpha$) and quantum numbers ($\beta$), and the integration is done over the whole space (spin included) leading to $\delta$ synonyms for Kronecker coefficients. The values of integrals that contribute to Eq. (28) are given in Eq. (12).

Let us now include the $j$-$j$ interaction,

$$\Xi\mathbf{J_1}\cdot\mathbf{J_2}=\Xi\frac{J^2-J_1^2-J_2^2}{2}. \tag{29}$$

We have to introduce three parameters to deal with antisymmetric coupling of two identical holes ($\Xi_0$ and $\Xi_2$) and coupling of the $J=3/2$ with the $J=1/2$ hole ($\Xi_1$). To take into account the crystal-field splitting $\xi J_z^2$, three parameters are also needed: $\xi_0$, $\xi_1$, and $\xi_2$. The first parameter, $\xi_0$, is needed when we deal with states $|\Gamma_6^{1\pm}\rangle$, $|\Gamma_5^{1\pm}\rangle$, and $|\Gamma_1^3\rangle$, arising from two identical holes $J=3/2$ whereas coupling of the $J=3/2$ with the $J=1/2$ hole leads to either states $|\Gamma_5^{3\pm}\rangle$ and $|\Gamma_1^5\rangle$ with total spin equal to 1 ($\xi_1$) or states $|\Gamma_6^{2\pm}\rangle$, $|\Gamma_5^{2\pm}\rangle$, and $|\Gamma_1^4\rangle$ with total spin equal to 2 ($\xi_2$).

In the basis of irreducible representations, the two-hole Hamiltonian writes

$$H_{\text{two-hole}}(\Gamma_1) = \begin{array}{c} \\ |\Gamma_1^1\rangle \\ |\Gamma_1^2\rangle \\ |\Gamma_1^3\rangle \\ |\Gamma_1^4\rangle \\ |\Gamma_1^5\rangle \end{array} \begin{array}{c} \begin{array}{ccccc} |\Gamma_1^1\rangle & |\Gamma_1^2\rangle & |\Gamma_1^3\rangle & |\Gamma_1^4\rangle & |\Gamma_1^5\rangle \end{array} \\ \begin{pmatrix} A_{11} - \frac{3}{4}\Xi_2 & 0 & 0 & 0 & A_{15} \\ 0 & A_{22} - \frac{15}{4}\Xi_0 & A_{23} & 0 & -\frac{A_{15}}{\sqrt{2}} \\ 0 & A_{23} & A_{22} - \frac{3}{4}\Xi_0 & 0 & \frac{A_{15}}{\sqrt{2}} \\ 0 & 0 & 0 & A_{44} + \frac{3}{4}\Xi_1 & 0 \\ A_{15} & -\frac{A_{15}}{\sqrt{2}} & \frac{A_{15}}{\sqrt{2}} & 0 & A_{44} - \frac{9}{4}\Xi_1 \end{pmatrix} \end{array} \tag{30}$$

for the two-hole states of $\Gamma_1$ symmetry,

$$H_{\text{two-hole}}(\Gamma_5) = \begin{array}{c} \\ |\Gamma_5^{1\pm}\rangle \\ |\Gamma_5^{2\pm}\rangle \\ |\Gamma_5^{3\pm}\rangle \end{array} \begin{array}{c} \begin{array}{ccc} |\Gamma_5^{1\pm}\rangle & |\Gamma_5^{2\pm}\rangle & |\Gamma_5^{3\pm}\rangle \end{array} \\ \begin{pmatrix} A_{22} - \frac{3\Xi_0}{4} + \xi_0 & \mp\frac{A_{15}}{2\sqrt{2}} & \mp\frac{\sqrt{3}A_{15}}{2\sqrt{2}} \\ \mp\frac{A_{15}}{2\sqrt{2}} & B_{22} + \frac{3\Xi_1}{4} + \xi_2 & \frac{\sqrt{3}A_{23}}{4} \\ \mp\frac{\sqrt{3}A_{15}}{2\sqrt{2}} & \frac{\sqrt{3}A_{23}}{4} & B_{33} - \frac{5\Xi_1}{4} + \xi_1 \end{pmatrix} \end{array} \tag{31}$$

for the two-hole states of $\Gamma_5$ symmetry, and

$$H_{\text{two-hole}}(\Gamma_6) = \begin{array}{c} \\ |\Gamma_6^{1\pm}\rangle \\ |\Gamma_6^{2\pm}\rangle \end{array} \begin{array}{c} \begin{array}{cc} |\Gamma_6^{1\pm}\rangle & |\Gamma_6^{2\pm}\rangle \end{array} \\ \begin{pmatrix} A_{22} - \frac{3}{4}\Xi_0 + 4\xi_0 & -\frac{A_{15}}{\sqrt{2}} \\ -\frac{A_{15}}{\sqrt{2}} & C_{22} - \frac{3}{4}\Xi_1 + 4\xi_2 \end{pmatrix} \end{array} \tag{32}$$

for the two-hole states of $\Gamma_6$ symmetry. In the equations above

$$A_{11} = 4\frac{\Delta_1 - \Delta_2 - 2\Delta_3}{3}, \tag{33}$$

$$A_{22} = 2\frac{2\Delta_1 + \Delta_2 + 2\Delta_3}{3}, \tag{34}$$

$$A_{23} = 2\frac{\Delta_1 + 2\Delta_2 - 2\Delta_3}{3}, \tag{35}$$

$$A_{44} = \Delta_1 - \Delta_2, \tag{36}$$

$$A_{15} = -\frac{\sqrt{2}(\Delta_1 - \Delta_2 + \Delta_3)}{3}, \tag{37}$$

$$B_{22} = \frac{7\Delta_1 - 4\Delta_2 - 2\Delta_3}{6}, \tag{38}$$

$$B_{33} = \frac{3}{2}\Delta_1 - \Delta_3, \tag{39}$$

$$C_{22} = \frac{5\Delta_1 + \Delta_2 - 4\Delta_3}{3}. \tag{40}$$

## IV. ACCEPTOR-BOUND EXCITON STATES AND SELECTION RULES FOR OPTICAL TRANSITIONS IN WURTZITE SEMICONDUCTORS

### A. Selection rules as predicted by group theory

The symmetry of the electron state is $\Gamma_7$. The coupling of the electron state with the two-hole $\Gamma_1$ states leads to $\Gamma_7$ states while $\Gamma_7 \otimes \Gamma_5$ and $\Gamma_7 \otimes \Gamma_6$ dissociate into $\Gamma_7 + \Gamma_9$ and $\Gamma_8 + \Gamma_9$, respectively.[17] Then, acceptor-bound exciton eigenstates have $\Gamma_7$, $\Gamma_8$, and $\Gamma_9$ symmetries.

The eigenvalues of the 30-fold acceptor-bound exciton problem (fortunately, the levels obey Kramers degeneracy, which leads to 15 twofold levels) in wurtzite semiconductors

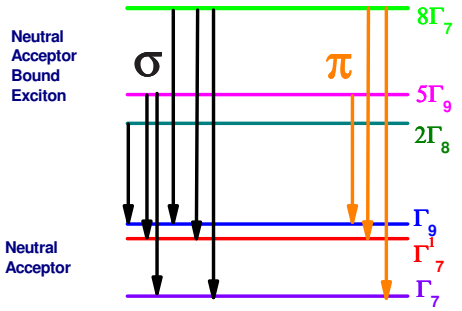


FIG. 2. (Color online) Summary of the optical transitions between neutral acceptor bound excitons and neutral acceptors in wurtzite semiconductors for $\sigma$ polarization ($\mathbf{E}\perp\mathbf{c}$) and $\pi$ polarization ($\mathbf{E}\|\mathbf{c}$). Ordering of levels is arbitrary.

can be solved by diagonalization of a block-diagonal Hamiltonian with an $8\times 8$ matrix for the eight twofold $\Gamma_7$ acceptor-bound exciton levels, a $5\times 5$ matrix for the twofold $\Gamma_9$ acceptor-bound exciton levels, and by analytical resolution of a $2\times 2$ Hamiltonian for the twofold $\Gamma_8$ levels. In an angular momentum representation, these states correspond to eigenvalues of the projection of their angular momentum being $\pm 1/2$, $\pm 3/2$, and $\pm 5/2$, respectively. Recombination of one hole with the electron in any of these 15 twofold states of the acceptor-bound exciton complex leads to one of the three neutral acceptor states as the final state. The final state is either the $\Gamma_9$ or one of the two $\Gamma_7$ acceptor states.

Radiative recombination of the $A_0^x\Gamma_8$ neutral acceptor-bound exciton in $\sigma(\mathbf{E}\perp\mathbf{c})$ polarization occurs with annihilation of the $\Gamma_7$ hole such as that the final neutral acceptor state is $\Gamma_9$. Radiative recombination of the $A_0^x\Gamma_9$ neutral acceptor-bound exciton states in $\sigma(\mathbf{E}\perp\mathbf{c})$ polarization occurs with annihilation of the $\Gamma_7$ hole such as that the final neutral acceptor state has $\Gamma_7$ symmetry. Finally, radiative recombination of $A_0^x\Gamma_7$ to any of the neutral acceptor states of $\Gamma_7$ symmetry is also allowed in $\sigma(\mathbf{E}\perp\mathbf{c})$ polarization via recombination of the $\Gamma_9$ hole. Group theory therefore predicts 36 transitions in $\sigma$ polarization.

In the context of $\pi(\mathbf{E}\|\mathbf{c})$, polarization radiative recombination occurs between acceptor-bound exciton and neutral acceptor states having identical symmetry. This gives five possibilities between initial and final states of $\Gamma_9$ symmetry and 16 possibilities between initial and final states of $\Gamma_7$ symmetry. This is summarized in Fig. 2. Of course, the possibility to resolve so many spectral lines is tributary to homogeneous and inhomogeneous broadening, accidental degeneracy, and thermalization effects if performing photoluminescence experiments, exciton-phonon interactions, and many other effects that distinguish solid-state physics from atomic physics.

### B. Acceptor-bound exciton eigenstates

Following Thomas and Hopfield's proposal[7] and in line with the procedure previously used for cubic crystals, acceptor-bound exciton states are described in terms of the coupling of the angular momentum of the two holes with the electron one. In the *j-j* coupling scheme, this is achieved by coupling the angular momentum of the two-hole state with the electron spin. The resulting states belong to the double group. A complete description requires an introduction of exchange-interaction term proportional to the scalar product $\mathbf{J}\cdot\boldsymbol{\sigma}$, where $\mathbf{J}$ is the two-hole state angular momentum and $\boldsymbol{\sigma}$ is the electron spin.

In terms of angular momentum algebra, we have the following states:

$$\Psi_{A+1/2}^{m_A+1/2} = \sqrt{\frac{A-m_A}{2A+1}}|m_A+1;-1/2\rangle + \sqrt{\frac{A+m_A+1}{2A+1}}|m_A;1/2\rangle, \tag{41}$$

$$\Psi_{A-1/2}^{m_A+1/2} = \sqrt{\frac{A+m_A+1}{2A+1}}|m_A+1;-1/2\rangle - \sqrt{\frac{A-m_A}{2A+1}}|m_A;1/2\rangle. \tag{42}$$

Using the language of angular momentum algebra, one would say that the absolute value of the projection of the angular momentum is a good quantum number.

#### 1. Acceptor-bound excitons with $\Gamma_8$ symmetry

The excitonic exchange interaction Hamiltonian writes

$$\begin{array}{cc} \left|\frac{5}{2},\pm\frac{5}{2}\right\rangle & \left|\frac{5}{2},\pm\frac{5}{2}\right\rangle' \\ \gamma_0 & 0 \\ 0 & \gamma_1 \end{array}, \tag{43}$$

where $\gamma_0$ and $\gamma_1$ are the two parameters required to distinguish the different nature of two-hole states having similar angular momentum value ($J=2$). Using Eq. (43), the global Hamiltonian and basis of acceptor-bound excitons with $\Gamma_8$ symmetry ($A_0^x\Gamma_8$) is expressed as

$$\begin{array}{cc} |\Gamma_6^{1\pm}\rangle\begin{pmatrix}\uparrow\\ \downarrow\end{pmatrix} & |\Gamma_6^{2\pm}\rangle\begin{pmatrix}\uparrow\\ \downarrow\end{pmatrix} \\ A_{22}-\frac{3}{4}\Xi_0+4\xi_0+\gamma_0 & -\frac{A_{15}}{\sqrt{2}} \\ -\frac{A_{15}}{\sqrt{2}} & C_{22}-\frac{3}{4}\Xi_1+4\xi_2+\gamma_1 \end{array} \tag{44}$$

with eigenvalues

$$E_8^{\mathrm{x}} = \frac{1}{2}\left[A_{22} + C_{22} - \frac{3}{4}(\Xi_0 + \Xi_1) + 4(\xi_0 + \xi_2) + \gamma_0 + \gamma_1\right] \pm \frac{1}{2}\left[\sqrt{\left\{A_{22} - C_{22} - \frac{3}{4}[\Xi_0 - \Xi_1] + 4(\xi_0 - \xi_2) + \gamma_0 - \gamma_1\right\}^2 + 2A_{15}^2}\right]. \tag{45}$$

Finally, introducing $A_{22}$, $A_{15}$, and $C_{22}$ from Eqs. (34), (37), and (40), we obtain

$$E_8^{\mathrm{x}} = \frac{1}{2}\left[3\Delta_1 + \Delta_2 - \frac{3}{4}(\Xi_0 + \Xi_1) + 4(\xi_0 + \xi_2) + \gamma_0 + \gamma_1\right] \pm \frac{1}{2}\left[\sqrt{\left\{\frac{-\Delta_1 + \Delta_2 + 8\Delta_3}{3} - \frac{3}{4}[\Xi_0 - \Xi_1] + 4(\xi_0 - \xi_2) + \gamma_0 - \gamma_1\right\}^2 + \frac{4(\Delta_1 - \Delta_2 + \Delta_3)^2}{9}}\right]. \tag{46}$$

### *2. Acceptor-bound excitons with $\Gamma_9$ symmetry*

In this case, the excitonic exchange-interaction Hamiltonian writes

| $\left\vert\frac{5}{2}, \pm\frac{3}{2}\right\rangle$ | $\left\vert\frac{5}{2}, \pm\frac{3}{2}\right\rangle'$ | $\left\vert\frac{3}{2}, \pm\frac{3}{2}\right\rangle_\alpha$ | $\left\vert\frac{3}{2}, \pm\frac{3}{2}\right\rangle'_\alpha$ | $\left\vert\frac{3}{2}, \pm\frac{3}{2}\right\rangle_\beta$ |
|---|---|---|---|---|
| $\gamma_0$ | 0 | 0 | 0 | 0 |
| 0 | $\gamma_1$ | 0 | 0 | 0 |
| 0 | 0 | $-\frac{3\gamma_0}{2}$ | 0 | 0 |
| 0 | 0 | 0 | $-\frac{3\gamma_1}{2}$ | 0 |
| 0 | 0 | 0 | 0 | $\frac{\gamma_2}{2}$ |

(47)

with

$$\left\vert\frac{5}{2}, \pm\frac{3}{2}\right\rangle = \frac{|\Gamma_6^{1\pm}\rangle\begin{pmatrix}\downarrow\\ \uparrow\end{pmatrix} + 2|\Gamma_5^{1\pm}\rangle\begin{pmatrix}\uparrow\\ \downarrow\end{pmatrix}}{\sqrt{5}}, \tag{48}$$

$$\left\vert\frac{5}{2}, \pm\frac{3}{2}\right\rangle' = \frac{|\Gamma_6^{2\pm}\rangle\begin{pmatrix}\downarrow\\ \uparrow\end{pmatrix} + 2|\Gamma_5^{2\pm}\rangle\begin{pmatrix}\uparrow\\ \downarrow\end{pmatrix}}{\sqrt{5}}, \tag{49}$$

$$\left\vert\frac{3}{2}, \pm\frac{3}{2}\right\rangle_\alpha = \frac{2|\Gamma_6^{1\pm}\rangle\begin{pmatrix}\downarrow\\ \uparrow\end{pmatrix} - |\Gamma_5^{1\pm}\rangle\begin{pmatrix}\uparrow\\ \downarrow\end{pmatrix}}{\sqrt{5}}, \tag{50}$$

$$\left\vert\frac{3}{2}, \pm\frac{3}{2}\right\rangle'_\alpha = \frac{2|\Gamma_6^{2\pm}\rangle\begin{pmatrix}\downarrow\\ \uparrow\end{pmatrix} - |\Gamma_5^{2\pm}\rangle\begin{pmatrix}\uparrow\\ \downarrow\end{pmatrix}}{\sqrt{5}}, \tag{51}$$

$$\left\vert\frac{3}{2}, \pm\frac{3}{2}\right\rangle_\beta = |\Gamma_5^{3\pm}\rangle\begin{pmatrix}\uparrow\\ \downarrow\end{pmatrix}. \tag{52}$$

From now on, the indices $\alpha$ and $\beta$ distinguish two-hole states based on the coupling of two identical holes, namely, with $J_1 = J_2 = 3/2$ ($\alpha$) from the two-hole states built from $J_1 = 3/2$ and $J_2 = 1/2$ holes ($\beta$). A third exchange-interaction parameter $\gamma_2$ is also introduced.

The $A_0^{\mathrm{x}}\Gamma_9$ states are solutions of the following Hamiltonian:

$$
\begin{array}{ccccc}
|\Gamma_5^{1\pm}\rangle\begin{pmatrix}\uparrow\\ \downarrow\end{pmatrix} & |\Gamma_5^{2\pm}\rangle\begin{pmatrix}\uparrow\\ \downarrow\end{pmatrix} & |\Gamma_5^{3\pm}\rangle\begin{pmatrix}\uparrow\\ \downarrow\end{pmatrix} & |\Gamma_6^{1\pm}\rangle\begin{pmatrix}\uparrow\\ \downarrow\end{pmatrix} & |\Gamma_6^{2\pm}\rangle\begin{pmatrix}\uparrow\\ \downarrow\end{pmatrix} \\
A_{22}-\dfrac{3\Xi_0}{4}+\xi_1+\dfrac{\gamma_0}{2} & \mp\dfrac{A_{15}}{2\sqrt{2}} & \mp\dfrac{\sqrt{3}A_{15}}{2\sqrt{2}} & \gamma_0 & 0 \\
\mp\dfrac{A_{15}}{2\sqrt{2}} & B_{22}+\dfrac{3\Xi_1}{4}+\xi_2+\dfrac{\gamma_1}{2} & \dfrac{\sqrt{3}A_{23}}{4} & 0 & \gamma_1 \\
\mp\dfrac{\sqrt{3}A_{15}}{2\sqrt{2}} & \dfrac{\sqrt{3}A_{23}}{4} & B_{33}-\dfrac{5\Xi_1}{4}+\xi_1+\dfrac{\gamma_2}{2} & 0 & 0 \\
\gamma_0 & 0 & 0 & A_{22}-\dfrac{3}{4}\Xi_0+4\xi_0-\gamma_0 & -\dfrac{A_{15}}{\sqrt{2}} \\
0 & \gamma_1 & 0 & -\dfrac{A_{15}}{\sqrt{2}} & C_{22}-\dfrac{3}{4}\Xi_1+4\xi_2-\gamma_1
\end{array}
\quad . \tag{53}
$$

There are no real simplifications to split this $(5\times5)$ system.

### *3. Acceptor-bound excitons with $\Gamma_7$ symmetry*

The excitonic exchange-interaction Hamiltonian writes

$$
\begin{array}{cccccccc}
\left|\frac{5}{2},\pm\frac{1}{2}\right\rangle & \left|\frac{5}{2},\pm\frac{1}{2}\right\rangle' & \left|\frac{3}{2},\pm\frac{1}{2}\right\rangle_\alpha & \left|\frac{3}{2},\pm\frac{1}{2}\right\rangle'_\alpha & \left|\frac{3}{2},\pm\frac{1}{2}\right\rangle_\beta & \left|\frac{1}{2},\pm\frac{1}{2}\right\rangle_\beta & \left|\frac{1}{2},\pm\frac{1}{2}\right\rangle_\gamma & \left[\frac{1}{2},\pm\frac{1}{2}\right) \\
\gamma_0 & 0 & 0 & 0 & 0 & 0 & 0 & 0 \\
0 & \gamma_1 & 0 & 0 & 0 & 0 & 0 & 0 \\
0 & 0 & -\dfrac{3\gamma_0}{2} & 0 & 0 & 0 & 0 & 0 \\
0 & 0 & 0 & -\dfrac{3\gamma_1}{2} & 0 & 0 & 0 & 0 \\
0 & 0 & 0 & 0 & \dfrac{\gamma_2}{2} & 0 & 0 & 0 \\
0 & 0 & 0 & 0 & 0 & -\gamma_2 & 0 & 0 \\
0 & 0 & 0 & 0 & 0 & 0 & 0 & 0 \\
0 & 0 & 0 & 0 & 0 & 0 & 0 & 0
\end{array}
\tag{54}
$$

with

$$
\left|\frac{5}{2},\pm\frac{1}{2}\right\rangle=\frac{\sqrt{2}|\Gamma_5^{1\pm}\rangle\begin{pmatrix}\downarrow\\ \uparrow\end{pmatrix}\pm\sqrt{3}|\Gamma_1^{3}\rangle\begin{pmatrix}\uparrow\\ \downarrow\end{pmatrix}}{\sqrt{5}}, \tag{55}
$$

$$
\left|\frac{5}{2},\pm\frac{1}{2}\right\rangle'=\frac{\sqrt{2}|\Gamma_5^{2\pm}\rangle\begin{pmatrix}\downarrow\\ \uparrow\end{pmatrix}+\sqrt{3}|\Gamma_1^{4}\rangle\begin{pmatrix}\uparrow\\ \downarrow\end{pmatrix}}{\sqrt{5}}, \tag{56}
$$

$$
\left|\frac{3}{2},\pm\frac{1}{2}\right\rangle_\alpha=\frac{\sqrt{3}|\Gamma_5^{1\pm}\rangle\begin{pmatrix}\downarrow\\ \uparrow\end{pmatrix}\mp\sqrt{2}|\Gamma_1^{3}\rangle\begin{pmatrix}\uparrow\\ \downarrow\end{pmatrix}}{\sqrt{5}}, \tag{57}
$$

$$
\left|\frac{3}{2},\pm\frac{1}{2}\right\rangle'_\alpha=\frac{\sqrt{3}|\Gamma_5^{2\pm}\rangle\begin{pmatrix}\downarrow\\ \uparrow\end{pmatrix}\mp\sqrt{2}|\Gamma_1^{4}\rangle\begin{pmatrix}\uparrow\\ \downarrow\end{pmatrix}}{\sqrt{5}}, \tag{58}
$$

$$
\left|\frac{3}{2},\pm\frac{1}{2}\right\rangle_\beta=\frac{|\Gamma_5^{3\pm}\rangle\begin{pmatrix}\downarrow\\ \uparrow\end{pmatrix}\pm\sqrt{2}|\Gamma_1^{5}\rangle\begin{pmatrix}\uparrow\\ \downarrow\end{pmatrix}}{\sqrt{3}}, \tag{59}
$$

$$
\left|\frac{1}{2},\pm\frac{1}{2}\right\rangle_\beta=\frac{\sqrt{2}|\Gamma_5^{3\pm}\rangle\begin{pmatrix}\downarrow\\ \uparrow\end{pmatrix}\mp|\Gamma_1^{5}\rangle\begin{pmatrix}\uparrow\\ \downarrow\end{pmatrix}}{\sqrt{3}}, \tag{60}
$$

$$\left|\frac{1}{2}, \pm\frac{1}{2}\right\rangle_{\gamma} = |\Gamma_1^2\rangle\begin{pmatrix}\uparrow\\ \downarrow\end{pmatrix}, \tag{61}$$

$$\left[\frac{1}{2}, \pm\frac{1}{2}\right) = [\Gamma_1^1\rangle\begin{pmatrix}\uparrow\\ \downarrow\end{pmatrix}. \tag{62}$$

The $A_0^x\Gamma_7$ states are solutions of an $8\times 8$ Hamiltonian

| $[\Gamma_1^1)\begin{pmatrix}\uparrow\\ \downarrow\end{pmatrix}$ | $\lvert\Gamma_1^2\rangle\begin{pmatrix}\uparrow\\ \downarrow\end{pmatrix}$ | $\lvert\Gamma_1^3\rangle\begin{pmatrix}\uparrow\\ \downarrow\end{pmatrix}$ | $\lvert\Gamma_1^4\rangle\begin{pmatrix}\uparrow\\ \downarrow\end{pmatrix}$ | $\lvert\Gamma_1^5\rangle\begin{pmatrix}\uparrow\\ \downarrow\end{pmatrix}$ | $\lvert\Gamma_5^{1\pm}\rangle\begin{pmatrix}\downarrow\\ \uparrow\end{pmatrix}$ | $\lvert\Gamma_5^{2\pm}\rangle\begin{pmatrix}\downarrow\\ \uparrow\end{pmatrix}$ | $\lvert\Gamma_5^{3\pm}\rangle\begin{pmatrix}\downarrow\\ \uparrow\end{pmatrix}$ |
|---|---|---|---|---|---|---|---|
| $A_{11}-\frac{3}{4}\Xi_2$ | 0 | 0 | 0 | $A_{15}$ | 0 | 0 | 0 |
| 0 | $A_{22}-\frac{15}{4}\Xi_0$ | $A_{23}$ | 0 | $-\frac{A_{15}}{\sqrt{2}}$ | 0 | 0 | 0 |
| 0 | $A_{23}$ | $A_{22}-\frac{3}{4}\Xi_0$ | 0 | $\frac{A_{15}}{\sqrt{2}}$ | $\sqrt{\frac{3}{2}}\gamma_0$ | 0 | 0 |
| 0 | 0 | 0 | $A_{44}+\frac{3}{4}\Xi_1$ | 0 | 0 | $\sqrt{\frac{3}{2}}\gamma_1$ | 0 |
| $A_{15}$ | $-\frac{A_{15}}{\sqrt{2}}$ | $\frac{A_{15}}{\sqrt{2}}$ | 0 | $A_{44}-\frac{9}{4}\Xi_1$ | 0 | 0 | $\sqrt{\frac{3}{2}}\gamma_2$ |
| 0 | 0 | $\sqrt{\frac{3}{2}}\gamma_0$ | 0 | 0 | $A_{22}-\frac{3\Xi_0}{4}+\xi_1-\frac{\gamma_0}{2}$ | $\mp\frac{A_{15}}{2\sqrt{2}}$ | $\mp\frac{\sqrt{3}A_{15}}{2\sqrt{2}}$ |
| 0 | 0 | 0 | $\sqrt{\frac{3}{2}}\gamma_1$ | 0 | $\mp\frac{A_{15}}{2\sqrt{2}}$ | $B_{22}+\frac{3\Xi_1}{4}+\xi_2-\frac{\gamma_1}{2}$ | $\frac{\sqrt{3}A_{23}}{4}$ |
| 0 | 0 | 0 | 0 | $\sqrt{\frac{3}{2}}\gamma_2$ | $\mp\frac{\sqrt{3}A_{15}}{2\sqrt{2}}$ | $\frac{\sqrt{3}A_{23}}{4}$ | $B_{33}-\frac{5\Xi_1}{4}+\xi_1-\frac{\gamma_2}{2}$ |

(63)

## V. COMPARISON WITH EXPERIMENTAL DATA

### A. Approximations

Determination of the identity of the recombination process illustrated by one or another photoluminescence feature is really an issue, which requires identification of the nature of both the initial and final states that may produce a given photon. Therefore, symmetry-breaking perturbations such as external uniaxial stresses or magnetic fields, which have been extensively used for acceptor-bound exciton studies in zinc-blende semiconductors may be of great help to solve this problem.[6] The complex theory built above can fortunately be simplified in the case of unstrained GaN, CdS, and ZnO. As we shall see later, the present model contradicts several earlier predictions in the literature. We take the GaN case to validate the simplification of the complex theory detailed in Secs. III and IV. This can be transferred to either CdS or ZnO, mutatis mutandis. The valence-band parameters of GaN have been taken as follows: $\Delta_1=10.2$ meV and $\Delta_2=\Delta_3=6$ meV (Table I). This gives hole energies of 16.2 meV($E_9$), 10.84 meV ($E_7^1$), and −6.64 meV ($E_7^2$). The valence-band parameters are also impacting the splitting of acceptor-bound exciton states through the coupling terms $A_{ij}$, $B_{ij}$, and $C_{ij}$. The difference in energy between acceptor-bound excitons and donor-bound excitons is typically about 5 meV in GaN.[19] In addition, the donor-bound exciton exhibits a series of narrow high-energy features corresponding to excited rotational states of the hole and to hydrogenic

TABLE I. Valence-band parameters ($\Delta_i$) and corresponding valence-band energies ($E_i$) for CdS, GaN, and ZnO.

| | CdS[a] | GaN[b] | ZnO[c] |
|---|---|---|---|
| $\Delta_1$ (meV) | 28 | 10.2 | 27.4 |
| $\Delta_2$ (meV) | 21 | 6 | 4.2 |
| $\Delta_3$ (meV) | 21 | 6 | 11.5 |
| $E_9$ (meV) | 49 | 16.2 | 31.6 |
| $E_1^7$ (meV) | 33.4 | 10.84 | 31.6 |
| $E_7^2$ (meV) | −26.4 | −6.64 | −8.4 |

[a]Reference 16.
[b]Reference 12.
[c]Reference 18.

excited states of electron. The valence-band structure calculation indicates that acceptor-bound exciton lines corresponding to excited states will be degenerate with the donor-bound exciton, free exciton, and the continuum. This statement also holds for CdS or ZnO. Thus, the sophisticated theory described in the preceding section can be restricted to states built from the coupling of two identical $J=3/2$ holes.

In the context of this approximation, the energy of the $A_0^X(\Gamma_8)$ state of interest for us, namely, $|\Gamma_6^{\pm}\rangle(\begin{smallmatrix}\uparrow\\ \downarrow\end{smallmatrix})$ is

$$A_0^X(\Gamma_8) = A_{22} - \frac{3}{4}\Xi_0 + 4\xi_0 + \gamma_0. \tag{64}$$

Introducing

$$E = A_{22} - \frac{3}{4}\Xi_0 + \gamma_0, \tag{65}$$

we re-write Eq. (64) as

$$A_0^X(\Gamma_8) = E + 4\xi_0. \tag{66}$$

The energies of the $\Gamma_9$ acceptor-bound excitons are obtained by resolution of the following $2\times 2$ Hamiltonian:

$$\begin{array}{cc} \dfrac{|\Gamma_6^{\pm}\rangle\begin{pmatrix}\downarrow\\ \uparrow\end{pmatrix} + 2|\Gamma_5^{\pm}\rangle\begin{pmatrix}\uparrow\\ \downarrow\end{pmatrix}}{\sqrt{5}} & \dfrac{2|\Gamma_6^{\pm}\rangle\begin{pmatrix}\downarrow\\ \uparrow\end{pmatrix} - |\Gamma_5^{\pm}\rangle\begin{pmatrix}\uparrow\\ \downarrow\end{pmatrix}}{\sqrt{5}} \\ A_{22} - \dfrac{3}{4}\Xi_0 + \dfrac{8}{5}\xi_0 + \gamma_0 & -\dfrac{6}{5}\xi_0 \\ -\dfrac{6}{5}\xi_0 & A_{22} - \dfrac{3}{4}\Xi_0 + \dfrac{17}{5}\xi_0 - \dfrac{3}{2}\gamma_0 \end{array} \tag{67}$$

whose solutions are analytical and given by

$$A_0^X(\Gamma_9)^{1,2} = A_{22} - \frac{3\Xi_0}{4} + \frac{5\xi_0}{2} - \frac{\gamma_0}{4} \pm \frac{1}{4}\sqrt{36\xi_0^2 - 36\xi_0\gamma_0 + 25\gamma_0^2}, \tag{68}$$

or

$$A_0^X(\Gamma_9)^{1,2} = E + \frac{5}{2}\xi_0 - \frac{5\gamma_0}{4} \pm \frac{1}{4}\sqrt{36\xi_0^2 - 36\xi_0\gamma_0 + 25\gamma_0^2}. \tag{69}$$

Concerning the four $\Gamma_7$ states, the corresponding $4\times 4$ Hamiltonian is

$$\begin{array}{cccc} [\Gamma_1^1)\begin{pmatrix}\uparrow\\ \downarrow\end{pmatrix} & [\Gamma_1^2)\begin{pmatrix}\uparrow\\ \downarrow\end{pmatrix} & [\Gamma_1^3)\begin{pmatrix}\uparrow\\ \downarrow\end{pmatrix} & [\Gamma_5^{\pm})\begin{pmatrix}\uparrow\\ \downarrow\end{pmatrix} \\ A_{11} - \dfrac{3}{4}\Xi_2 & 0 & 0 & 0 \\ 0 & A_{22} - \dfrac{15}{4}\Xi_0 & A_{23} & 0 \\ 0 & A_{23} & A_{22} - \dfrac{3}{4}\Xi_0 & \sqrt{\dfrac{3}{2}}\gamma_0 \\ 0 & 0 & \sqrt{\dfrac{3}{2}}\gamma_0 & A_{22} - \dfrac{3}{4}\Xi_0 + \xi_1 - \dfrac{\gamma_0}{2} \end{array} \tag{70}$$

which gives a trivial eigenvalue $A_{11}-\frac{3}{4}\Xi_2$ (it corresponds to spin-orbit split hole states) and the eigenvalues of the $3\times 3$ matrix below

$$\begin{pmatrix} E - 3\Xi_0 - \gamma_0 & A_{23} & 0 \\ A_{23} & E - \gamma_0 & \sqrt{\dfrac{3}{2}}\gamma_0 \\ 0 & \sqrt{\dfrac{3}{2}}\gamma_0 & E + \xi_1 - \dfrac{3}{2}\gamma_0 \end{pmatrix}. \tag{71}$$

### B. CdS

This is the most documented situation in terms of fine structure of the acceptor-bound exciton state in wurtzite semiconductors. The main acceptor-bound exciton emission line $I_1$ in CdS occurs at 2.5356 eV.[8] In earlier absorption measurements, a high-energy replica of the $I_1$ line is obtained (2.53595 eV).[7] In both cases, the line is strongly $\mathbf{E}\perp\mathbf{c}$ polarized and is attributed to a transition from the acceptor-bound exciton ($A_0^X$) ground state to the $\Gamma_9$ state of the neutral acceptor. At this stage, our theory indicates that the $A_0^X$ ground state has either $\Gamma_8$ or $\Gamma_7$ symmetry.

In addition to the $I_1$ line, a number of high-energy peaks related to the $A_0^X$ have been observed in absorption[7] and photoluminescence excitation spectra.[8] The $\mathbf{E}\|\mathbf{c}$ polarized excitation spectrum of $I_1$ revealed four resonances at 2.5479 eV ($I_{1B}^1$), 2.5485 eV ($I_{1B}^2$), 2.5494 eV ($I_{1B'}^1$), and 2.5500 eV ($I_{1B'}^2$).[8] The two strongest resonances $I_{1B}^1$ and $I_{1B'}^2$ (presumably $\mathbf{E}\|\mathbf{c}$ polarized) were interpreted as $A_0^X(\Gamma_9)\rightarrow\Gamma_9$ transitions. The other two weaker resonances $I_{1B}^2$ and $I_{1B'}^1$ are attributed to transitions involving $A_0^X(\Gamma_8)$ and $A_0^X(\Gamma_7)$ states, respectively. These transitions are in first order allowed only for $\mathbf{E}\perp\mathbf{c}$ polarization but also observed in $\mathbf{E}\|\mathbf{c}$ polarized spectra due to the high excitation used.[8] In the $\mathbf{E}\perp\mathbf{c}$ polarized excitation spectra, up to 12 lines are resolved within the energy region located 6–7 meV above of the $I_1$ line. These lines (except for the two closest to $I_1$ lines: $I_1^1$ at 2.5381 eV and $I_1^2$ at 2.5393 eV) were identified as excited electronic and vibronic states of the acceptor-bound exciton. The $I_1^1$ and $I_1^2$ lines were interpreted as $\Gamma_9\rightarrow A_0^X(\Gamma_8)$ transitions where the $A_0^X(\Gamma_8)$ state involves two identical $J=3/2$ holes with parallel spins.[8] However, such a state is Pauli forbidden and the above interpretation is questionable.

Thomas and Hopfield[7] reported two high-energy absorption lines of $A_0^X$, labeled $I_{1B}$ and $I_{1B'}$. The $I_{1B'}$ line at 2.5504 eV seen only for $\mathbf{E}\|\mathbf{c}$ polarization corresponds to the $I_{1B'}^2$ line in Ref. 8 (both are separated by 14.4 meV from the $I_1$ line). The $I_{1B}$ line appeared at 2.54887 eV for $\mathbf{E}\|\mathbf{c}$ polarization and at 2.54914 eV for $\mathbf{E}\perp\mathbf{c}$ polarization. It seems that the two $I_{1B}$ components corresponds to the $I_{1B}^1$ and $I_{1B}^2$ lines reported by Baumert *et al.*[8] but the splitting between them as well as their separation from the $I_1$ line are different in the two papers. (We should note that the data of Thomas and Hopfield[7] are not cited correctly in Table II in Ref. 8). Another discrepancy concerns the $\mathbf{E}\perp\mathbf{c}$ polarized $I_{1B'}^1$ line[8] which in Ref. 7 is labeled $I_3$ and interpreted as due to ionized donor-bound exciton based on the observed splitting pattern in magnetic field.

We note that slight strain effects correlated with the way samples are mounted on the sample holder may impact the transitions energies, eventually break the crystal point symmetry and lead to impure selection rules. These discrepancies among experimental papers are really acceptable.

Thanks to the theory developed above, we are able to more properly describe the experimental data for the $A_0^X$ absorption/recombination and to make a quantitative analysis of the expected splitting energies. Considering only the lowest-energy levels of the $A_0^X$ (formed by two $J=3/2$ holes), six optical transitions (all doubly degenerate) to the $\Gamma_9$ acceptor state are possible: four for $\mathbf{E}\perp\mathbf{c}$ polarization and two for $\mathbf{E}\|\mathbf{c}$ polarization.

In our interpretation, the ground state of the $A_0^X$ (involved in $I_1$ absorption/recombination line) has $\Gamma_7$ symmetry. The two $\mathbf{E}\|\mathbf{c}$ polarized lines observed at 12.9 meV (Ref. 7) [12.3 meV (Ref. 8)] and 14.4 meV above the $I_1$ line correspond to the two $A_0^X(\Gamma_9)\rightarrow\Gamma_9$ transitions. According to Eq. (69), the energy splitting $\Sigma$ between the two lines is given by

$$\sum = \frac{1}{2}\sqrt{36\xi_0^2 - 36\xi_0\gamma_0 + 25\gamma_0^2}. \tag{72}$$

This equation gives an elliptic relation between $\xi_0$ and $\gamma_0$,

$$\frac{[2\xi_0-\gamma_0]^2}{\left(\frac{2\Sigma}{3}\right)^2} + \frac{\gamma_0^2}{\left(\frac{\Sigma}{2}\right)^2} = 1. \tag{73}$$

In CdS, the experimentally determined splitting $\Sigma = 1.5$ meV. Inserting the experimental value into Eq. (73), one gets

$$\xi_0 = \frac{\gamma_0}{2} \pm \sqrt{\left(\frac{1}{2}\right)^2 - \left(\frac{2}{3}\gamma_0\right)^2}. \tag{74}$$

The physical solutions for Eq. (74) dictate the following inequality to be fulfilled $|\gamma_0| \leq \frac{3}{4}$ meV, further leading to $|\xi_0| \leq \frac{5}{8}$ meV. It is worthwhile noticing that both values of $\xi_0$ and $\gamma_0$ are on the order of 1 meV, at most. Therefore, the splitting between line $I_1$ and the other transitions is ruled by the value of $\Xi_0$. The experimental splitting $I_1 - \langle A_0^x(\Gamma_9)\rangle$ between the center of gravity $\langle A_0^x(\Gamma_9)\rangle$ of lines associated to $A_0^X(\Gamma_9)\rightarrow\Gamma_9$ recombination and $I_1$ is 13.6 meV. This leads us to write

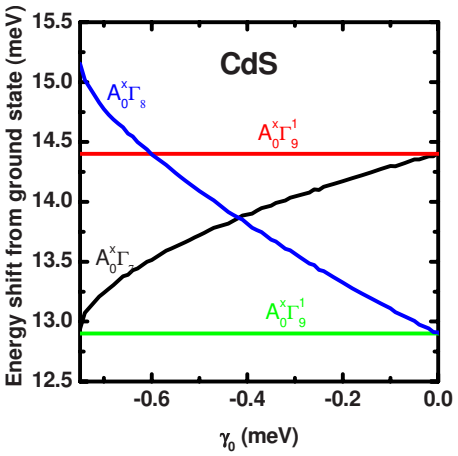


FIG. 3. (Color online) Plot of the transition energies relative to the ground-state photoluminescence lines in CdS for different values of the short-range electron-hole exchange interaction.

$$I_1 - \langle A_0^x(\Gamma_9)\rangle = 3\Xi_0 - \frac{A_{23}^2}{3\Xi_0} - \frac{\gamma_0}{4} = 13.6 \text{ meV}. \tag{75}$$

A simple calculation with $A_{23}=19$ meV leads to the following estimate: $\Xi_0 \approx 4.0$ meV.

We have then performed the final fitting of the value $\gamma_0$ using matrix diagonalization rather than perturbation theory since $A_{23}=19$ meV is not so small a matrix element, compared to diagonal terms.

An additional indicator for choosing the set of parameters that fit the data is the experimental report of two transitions optically active in $\sigma$ polarization at energies intermediate between the recombination energies of the two $A_0^X(\Gamma_9)$ excitons. Selection rules do not help us in establishing the symmetry of these acceptor-bound excitons; they are $\Gamma_7$ or $\Gamma_8$ irreducible representations of $C_{6v}$.

The fit to the data is shown in Fig. 3 where are plotted the energy difference between the ground-state PL energy and the high-energy lines. The whole set of data interprets in the context of a large value of the short-range hole-exchange interaction $\Xi_0 \sim 3.4$ meV. The physical values of the electron-hole spin-exchange interaction, a negative quantity, is in the $-0.4 \pm 0.1$ meV range and the crystal-field splitting of the two-hole state is about $0.2 \pm 0.1$ meV. This leads to $\Xi_0 \sim 3.4 \pm 0.2$ meV. The sequence of levels for the six first levels, in terms of increasing recombination energy, is either $A_0^X(\Gamma_7)$, $A_0^X(\Gamma_9)$, $A_0^X(\Gamma_7)$, $A_0^X(\Gamma_8)$, $A_0^X(\Gamma_9)$, $A_0^X(\Gamma_7)$ or $A_0^X(\Gamma_7)$, $A_0^X(\Gamma_9)$, $A_0^X(\Gamma_8)$, $A_0^X(\Gamma_7)$, $A_0^X(\Gamma_9)$, $A_0^X(\Gamma_7)$, depending on the value of $\gamma_0$. It is worthwhile noticing that the crystal-field splitting parameter is obtained according to the solution having sign plus in Eq. (75). Using sign minus leads to solutions with similar values of $\gamma_0$ but with their signs changed. We believe the positive value not to be of physical meaning. In Fig. 4 are plotted the values of $\Xi_0$ versus the whole set of $\gamma_{0s}$ allowed by Eq. (75). Solutions compatible with the experiment correspond to the left-hand bottom part of the closed curve which is indicated by the bended arrow.

A plot of the evolution of $A_0^X(\Gamma_8)$ energy levels versus $\gamma_0$ leads to an elliptic graph, which is not a surprise, in relation

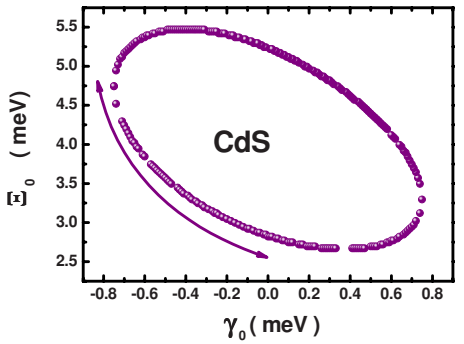


FIG. 4. (Color online) Plotted values of $\Xi_0$ versus the whole set of $\gamma_0$'s allowed by Eq.(75). Solutions compatible with the experiment correspond to the left-hand bottom part of the close curve which is indicated by the bended arrow.

with Eqs. (66) and (75). A quarter of this curve is plotted in Fig. 3. A similar behavior is also observed for level $A_0^X(\Gamma_7^2)$. The ordering of $A_0^X(\Gamma_8)$ and $A_0^X(\Gamma_7^2)$ versus $\gamma_0$ is symmetric with respect to the long axis of the ellipsoids that represent evolution of $A_0^X(\Gamma_8)$ and $A_0^X(\Gamma_7^2)$ levels.

It is worthwhile noticing that the symmetry of the acceptor-bound exciton associated with $I_1$ recombination line is written $|\frac{1}{2},\pm\frac{1}{2}\rangle$ in terms of total angular momentum representation. This situation is opposite to the one encountered for acceptor-bound excitons in cubic crystals where the level ordering is $|\frac{5}{2},\pm\frac{m_{5/2}}{2}\rangle$, $|\frac{3}{2},\pm\frac{m_{3/2}}{2}\rangle$, $|\frac{1}{2},\pm\frac{1}{2}\rangle$ in terms of recombination energies. The value of $\Xi_0$ we report here reverses the symmetry of the acceptor-bound excitons compared with cubic semiconductors. This difference is, we believe in essence, correlated with band-structure effects typical of wurtzitic semiconductors on the one hand, and on the other hand correlated with the valence-band dispersion which is flatter, giving higher hole masses and smaller acceptor Bohr radii in wide-band-gap semiconductors and leading to high values of the hole-hole exchange interaction. The electron-hole spin-exchange interaction is about $-0.4\pm0.1$ meV, a value comparable to the short-range exchange interaction for free excitons.[16] Calculating it would be a very difficult issue but we are able to compare the relative values of $\Xi_0$ and $\gamma_0$ in the context of the effective-mass argument. For holes having large effective masses, the direct Coulomb repulsion between two holes is stronger than the direct Coulomb attraction between the electron and the two holes, thanks to the light value of the electron mass compared with the hole one. This argument also holds for the exchange parts of the Coulomb interactions.

In zinc-blende semiconductors, InP and GaAs, the hole mass is also heavier than the electron one but the differences are not so drastic. Both the hole-hole and electron-hole exchange interactions equal typically 0.2 meV for acceptor-bound exciton,[6] giving at the end, a less clear picture and no resolution of the fine-structure splitting of $|\frac{5}{2},\pm\frac{m_{5/2}}{2}\rangle$ and $|\frac{3}{2},\pm\frac{m_{3/2}}{2}\rangle$ acceptor states.

### C. GaN

In the case of GaN, existence of two kinds of acceptors was predicted.[20,21] One kind is the general (effective mass) acceptor such as C substitutes N and other kind includes Mg, Zn, and Cd which properties slightly deviate from those expected by the effective-mass theory. In wurtzite GaN, two acceptors have been studied in low-temperature PL with sufficient spectral resolution to allow a discussion of the splitting of $A_0^X$ states. The shallowest $A_0^X$ state has a PL line at about 3.466 eV in unstrained GaN.[22] Its origin is an Mg-related acceptor,[23] stable in *n*-GaN and having interesting properties in *p*-GaN (instability and metastability[19]). The acceptor ground state appears to be approximately effective-masslike, with a strong anisotropy of the bound hole *g* tensor.[19,24] In material of sufficiently low doping, a second emission line of the $A_0^X$, 0.8 meV lower in energy is also resolved. The doublet structure was tentatively interpreted as due to the internal coupling in the $A_0^X$ complex.[22] In contrast, from their magneto-PL studies, Stepniewski *et al.*[25] suggested that the two components of the $A_0^X$ emission do not arise from the splitting of the initial state but from the neutral acceptor ground state instead. Such a conclusion comes from the analysis of the Zeeman splitting patterns at different angles between magnetic field orientation and the crystal *c* axis. However, in order to obtain a satisfactory fit of the data within quasicubic model, the authors assumed a spin-orbit interaction $\Delta_{so}=3\Delta_2(=3\Delta_3)$ for the hole bound to acceptor of 1.3 meV as compared to $\Delta_{so}=18$ meV for the free hole. In fact, a decrease in the spin-orbit interaction for effective-mass acceptor in GaN by a factor up to about 0.67 has been predicted by the theory.[26] The huge reduction as suggested in Ref. 25 seems to be unlikely, however. Moreover, even in the case of very small splitting between the two acceptor states, the transition from the $A_0^X$ ground state to the $\Gamma_7$ acceptor state should occur at a higher energy than that to the $\Gamma_9$ acceptor state, which contradicts with the above interpretation. Then, we are bound to believe that the two PL lines of the Mg-related $A_0^X$ correspond to a splitting of the initial state, i.e., of the $A_0^X$ itself.

The other case where resolved PL lines for the $A_0^X$ state have been reported is the Zn acceptor in GaN. Zn introduces a deep acceptor in GaN, with a binding energy about 0.34 eV.[27] The *g* tensor for the bound hole in the acceptor ground state is quite isotropic, as expected for a deep acceptor state.[28] This acceptor has an $A_0^X$ PL spectrum consisting of three resolved lines at 3.4542, 3.4546, and 3.4556 eV in strain-free GaN crystals at 2 K.[27] Variable temperature measurements showed an increased intensity of the high-energy lines relative to that of the 3.4542 eV line with increasing temperature, implying a splitting in the $A_0^X$ complex.[29] No magneto-PL data have been presented for the Zn acceptor case, to our knowledge.

Due to the limited experimental data available, the analysis of the fine structure of $A_0^X$ state in GaN is quite difficult. Since the PL measurements discussed above were performed with detection along the *c* axis, we can assume that all $A_0^X$ recombination lines correspond to transitions with a predominant $\sigma$ polarization. As in the case of CdS, the ground-state acceptor exciton is believed to have $\Gamma_7$ symmetry and the strongest PL lines (3.466 and 3.4542 eV for Mg- and Zn-related complexes, respectively) are interpreted as $A_0^X(\Gamma_7^1)\rightarrow\Gamma_9$ transitions. Then, the two higher-energy lines for Zn-related $A_0^X$ should correspond to $A_0^X(\Gamma_8)\rightarrow\Gamma_9$ and

$A_0^X(\Gamma_7) \rightarrow \Gamma_9$ transitions. The ordering of $A_0^X(\Gamma_8)$ and $A_0^X(\Gamma_7)$ is not clear *a priori.*

In the case of Mg-related $A_0^X$, the low-energy PL line is difficult to explain if the transition is still toward $\Gamma_9$ acceptor states, some of $\Gamma_8$ and $\Gamma_7^3$ states should be below the $\Gamma_7^1$. We can speculate that this is $A_0^X(\Gamma_9)^1 \rightarrow \Gamma_7$ transition (only one possible for $\sigma$ polarization). In such a case, we get $A_0^X(\Gamma_9)^1 - A_0^X(\Gamma_7)^1$ splitting of 6.16 meV for the nonperturbed separation between the $\Gamma_9$ and $\Gamma_7$ acceptor states (i.e., without reduction in the spin-orbit interaction).

This is the current experimental situation for the physical structure of acceptor-bound excitons in GaN.

## VI. CONCLUSIONS

We have described the internal structure of acceptor-bound excitons in wurtzite semiconductors, using angular momentum algebra in the context of invariants' theory. Our approach consisted in first constructing the wave functions of the two-hole system which fulfill Pauli's exclusion's principle. Then, we constructed the acceptor-bound exciton states by adding the electron states in a similar manner as the two-hole states were constructed. We discussed the optical selection rules for the acceptor-bound exciton recombination. We compared our theory with experimental data for CdS and GaN.

In the specific case of CdS, for which much experimental information is available we demonstrated that the sign of the short-range hole-exchange interaction is reversed compared with cubic semiconductors. We have shown that the arithmetic value of this exchange interaction is more than one order of magnitude larger than that in zinc-blende semiconductors. The whole set of data interprets in the context of a large value of the short-range hole-exchange interaction $\Xi_0 = 3.4 \pm 0.2$ meV. This value dictates the splitting between the ground-state line $I_1$ and the other transitions. Values we find of the electron-hole spin-exchange interaction and of the crystal-field splitting of the two-hole state are $\gamma_0 = -0.4 \pm 0.1$ meV and $\xi_0 = 0.2 \pm 0.1$ meV, respectively. The sequence of levels is in terms of increasing recombination energy: $A_0^X(\Gamma_7)$, $A_0^X(\Gamma_9)$, $A_0^X(\Gamma_7)$, $A_0^X(\Gamma_8)$, $A_0^X(\Gamma_9)$, and $A_0^X(\Gamma_7)$.

In case of GaN, the experimental data for the acceptor-bound excitons in the case of Mg and Zn acceptors, show splitting into more than one bound-exciton ground state. We discussed a possible assignment of these states but could not fit the three parameters of our model due to observation of three lines (two splittings) only.


[1] P. J. Dean and D. C. Herbert, in *Excitons*, edited by K. Cho (Springer, Berlin, 1979), p. 55.

[2] *Confined Electrons and Photons*, NATO Advanced Studies Institute, Series B: Physics Vol. 340, edited by E. Burstein and C. Weisbuch (Plenum, New York, 1995).

[3] E. U. Condon and G. H. Shortley, *Theory of Atomic Spectra* (Cambridge University Press, Cambridge, 1963).

[4] B. Gil, P. Bigenwald, M. Leroux, P. P. Paskov, and B. Monemar, Phys. Rev. B **75**, 085204 (2007).

[5] B. Monemar, P. P. Paskov, J. P. Bergman, A. A. Toropov, T. V. Shubina, T. Malinauskas, and A. Usui, Phys. Status Solidi B **245**, 1723 (2008).

[6] H. Mathieu, J. Camassel, and F. B. Chekroun, Phys. Rev. B **29**, 3438 (1984), and references therein.

[7] D. G. Thomas and J. J. Hopfield, Phys. Rev. **128**, 2135 (1962).

[8] R. Baumert, I. Broser, J. Gutowski, and A. Hoffmann, Phys. Rev. B **27**, 6263 (1983).

[9] G. E. Pikus and L. G. Bir, *Symmetry and Strain-Induced Effects in Semiconductors* (John Wiley and Sons, New York, 1974).

[10] K. Cho, Phys. Rev. B **14**, 4463 (1976).

[11] R. Dingle, D. D. Sell, S. E. Stokowski, and M. Ilegems, Phys. Rev. B **4**, 1211 (1971).

[12] B. Gil, O. Briot, and R. L. Aulombard, Phys. Rev. B **52**, R17028 (1995).

[13] B. Gil, F. Hamdani, and H. Morkoç, Phys. Rev. B **54**, 7678 (1996).

[14] M. E. Rose, *Elementary Theory of Angular Momentum* (John Wiley and Sons, New York, 1957).

[15] R. N. Zare, *Angular Momentum* (John Wiley and Sons, New York, 1988).

[16] *Semiconductors: Group IV Elements and III-V Compounds*, Data in Science and Technology, edited by O. Madelung (Springer, Berlin, 1991); *Semiconductors: Other Than Group IV Elements and III-V Compounds*, Data in Science and Technology, edited by O. Madelung (Springer, Berlin, 1991).

[17] *The Properties of the Thirty-Two Point Groups*, edited by G. F. Koster, J. O. Dimmock, R. G. Wheeler, and H. Statz (MIT, Cambridge, 1963).

[18] B. Gil, A. Lusson, V. Sallet, S.-A. Said-Hassani, R. Triboulet, and P. Bigenwald, Jpn. J. Appl. Phys., Part 2 **40**, L1089 (2001).

[19] B. Monemar, P. P. Paskov, G. Pozina, C. Hemmingsson, J. P. Bergman, T. Kawashima, H. Amano, I. Akasaki, T. Paskova, S. Figge, D. Hommel, and A. Usui, Phys. Rev. Lett. **102**, 235501 (2009).

[20] G. D. Chen, M. Smith, J. Y. Lin, H. X. Jiang, Su-Huai Wei, M. Asif Khan, and C. J. Sun, Appl. Phys. Lett. **68**, 2784 (1996).

[21] Jian-Bai Xian, K. W. Cheah, Xiao-Liang Wang, Dian-Zhao Sun, and Mei-Ying Kong, Phys. Rev. B, **59**, 10119, (1999).

[22] K. Kornitzer, T. Ebner, K. Thonke, R. Sauer, C. Kirchner, V. Schwegler, M. Kamp, M. Leszczynski, I. Grzegory, and S. Porowski, Phys. Rev. B **60**, 1471 (1999).

[23] L. Chen and B. J. Skromme, Mater. Res. Soc. Symp. Proc. **743**, L11.35 (2003).

[24] E. R. Glaser, M. Murthy, J. A. Freitas, Jr., D. F. Storm, L. Zhou, and D. J. Smith, Physica B **401-402**, 327 (2007).

[25] R. Stepniewski, A. Wysmolek, M. Potemski, K. Pakula, J. M. Baranowski, I. Grzegory, S. Porowski, G. Martinez, and P. Wyder, Phys. Rev. Lett. **91**, 226404 (2003).

[26] A. V. Malyshev, I. A. Merkulov, and A. V. Rodina, Phys. Solid State **40**, 917 (1998).

[27] B. Monemar, H. P. Gislason, and O. Lagerstedt, J. Appl. Phys. **51**, 640 (1980).

[28] M. Kunzer, A. Baur, U. Kaufmann, J. Schneider, H. Amano, and I. Akasaki, Solid-State Electron. **41**, 189 (1997).

[29] B. J. Skromme, K. C. Palle, C. D. Poweleit, H. Yamane, M. Aoki, and F. J. DiSalvo, Appl. Phys. Lett. **81**, 3765 (2002).